Mechanical Design, Planning, and Control for Legged Robots in Distillation Columns

Tamas G. Molnar*
California Institute of Technology
Pasadena, California, 91125, USA
e-mail: tmolnar@caltech.edu

Katherine Tighe*
NASA Jet Propulsion Laboratory
California Institute of Technology
Pasadena, California, 91109, USA
e-mail: katherine.c.tighe@jpl.nasa.gov

Wyatt Ubellacker
California Institute of Technology
Pasadena, California, 91125, USA
e-mail: wubellac@caltech.edu

Arash Kalantari
NASA Jet Propulsion Laboratory
California Institute of Technology
Pasadena, California, 91109, USA
e-mail: arash.kalantari@jpl.nasa.gov

Aaron D. Ames
California Institute of Technology
Pasadena, California, 91125, USA
e-mail: ames@caltech.edu

Dexterous robots have great potential to execute industrial tasks that are not suited to humans. In this work, a novel robotic mobility platform is proposed for use in the chemical industry to enable autonomous distillation column inspection — a tedious and dangerous task for humans. A roller arm mechanism is designed for a quadrupedal robot that enables moving across the distillation column. Required dynamic behaviors are generated with full-body motion planning and low-level control. The holistic process of mechanical design, planning, and control leads to desired behavior, as demonstrated by high-fidelity simulations. This marks a key step towards operating legged robots inside distillation columns.

1 INTRODUCTION

Robotics and automation continue to revolutionize industry. Robots can operate in environments where it is impossible, dangerous or unhealthy for humans to work, or execute tasks that are difficult, uncomfortable or monotonous for humans [1, 2]. Examples include search and rescue [3], manufacturing [4, 5], and work in chemical industry [6], just to mention a few. These tasks may require skillful, agile motions and a variety of behaviors from the robots, which creates the need for unique robot designs and sophisticated algorithms to operate them.

This paper presents a complete design process for a novel robotic system—from mechanical design to planning and control—that enables unique behaviors and capabilities in the context of inspecting complex industrial spaces; specifically, chemical distillation columns. The process is indicative of a general approach that holistically considers mechanical design and control, with potential to endow robots with novel dynamic behaviors and thereby enable unique, complex tasks. There exist inspiring works that address the whole spectrum of design and computation. These include rehabilitation robots [7], humanoid robots [8], quadrupeds [9, 10, 11, 12] and systems mounted on robots such as manipulator arms [13]. To our knowledge, our work is the first example of the end-to-end design process in a complex industrial application.

*These authors contributed equally. K. Tighe led the mechanical design and T. G. Molnar led the computation and simulation.

1.1 Overview of Problem and Proposed Solution

In this paper, we develop a robotic mobility platform and its dynamic behaviors for application in the chemical industry: we aim to utilize legged robots to inspect distillation columns. As the primary equipment in the chemical process industries [14], distillation columns are made up of a series of stacked round trays with a diameter of up to six meters and a total height of up to 60 meters. The interiors of these columns require routine visual and physical inspection to look for signs of damage, fouling, corrosion or mechanical issues including displaced or stuck valves, bent, cracked, or displaced trays, loose or missing bolts, etc. Currently, trained personnel have to perform this tedious task by spending several hours inside the column which can expose them to great health risks of working in a confined and contaminated environment and danger of falling from heights. Instead of exposing personnel to such risks, we develop a semi-autonomous, compliant-legged robotic solution to climb up and down inside distillation columns while inspecting the column.

The development of this mobility system is summarized in Fig. 1. Apart from operating in tight spaces, a key challenge for the robot is to transition (climb up or down) across the trays of the distillation column, which is the focus of this paper. Successful transition necessitates a unique mechanical design to make it physically possible, as well as motion planning and control to synthesize the required dynamic behavior. The solution must be robust to various distillation column specifications (including manway width and length and tray spacing), while eliminating the risk of free fall of the robot. Additionally, the design must be light and compact enough to not exceed the available payload of the mobility platform.

There exist robotic systems in the literature that are capable of similar dynamic behaviors to the ones required for distillation column inspection. On one hand, several works addressed legged locomotion in challenging environments, such as in confined spaces [15], over obstacles and rough terrain [16, 17, 18, 19, 20], and on stepping stones [21, 22, 23]. On the other hand, there exist robotic systems capable of climbing, including bio-inspired designs [24, 25, 26] and soft robots [27]. As such, [28] traversed through cables with brachiating robots, [29] made quadrupeds climb poles, [30] used special grippers on quadrupeds to climb vertical ladders, and [31] proposed a six legged limb mechanism to climb on parallel walls.

The solutions above, however, are specific to their main mobility platforms and target environments, and cannot be applied for our purpose. To the best of our knowledge, there is no existing legged platform capable of moving up and down in distillation columns. To fill this gap, we propose a novel solution.

1.2 Contributions

A robotic system is developed that is able to explore the inside of a distillation column by navigating around on trays and climbing up and down between trays through manways while carrying an inspection sensor payload.

This goal is achieved by two contributions. First, we propose a roller arm design for an off-the-shelf Unitree A1 quadrupedal robot that enables versatile dynamic behaviors, including transition between the levels of the distillation column. We describe the design ideation, selection and iteration process, as well as the final design with its actuators and feasible ranges of motion (see Section 2). Second, we incorporate the model of the robot with the roller arm into a full-body dynamic motion planner, and generate trajectories for transitioning between trays by solving an optimization problem. We employ low-level tracking controllers to follow the dynamically feasible trajectories generated by the motion planner and execute the transition (Section 3). The overarching process of mechanical design, motion planning, and control culminates in successful tray transition both up and down the distillation column, that is demonstrated by high-fidelity simulation (Section 4). This achieves a key step towards realizing distillation column inspection by legged robots, which is otherwise a dangerous and tedious task for humans.

2 MECHANISM AND MECHANICAL DESIGN

In this section, we describe the mechanical design process to create the robotic mobility platform, capable of both moving around on a tray and climbing up and down between trays. We chose a quadrupedal robot (Unitree A1) as the base mobility platform and designed a novel add-on four-degrees-of-freedom arm (Roller Arm) to help the robot climb up and down inside the column. The most important parameters, driving the design and selection of the mobility system, are the ranges of distillation column dimensions, detailed in Table 1 and Fig. 2. Further requirements include the ability to traverse up and down the column with low risk of falling while being robust to external disturbances; using no external system (like cable or elevator) for transition between trays; being agnostic to the alignment of the manways; being functional with or without tethered connection to a base station; and payload capacity to carry navigation and inspection systems.

2.1 Roller Arm Mechanism

Once design requirements were defined, potential concepts for the transition mechanism were generated. The identified concepts are categorized in three groups:

- Freeform: the robot goes through a period of unconstrained motion where it is not touching any part of

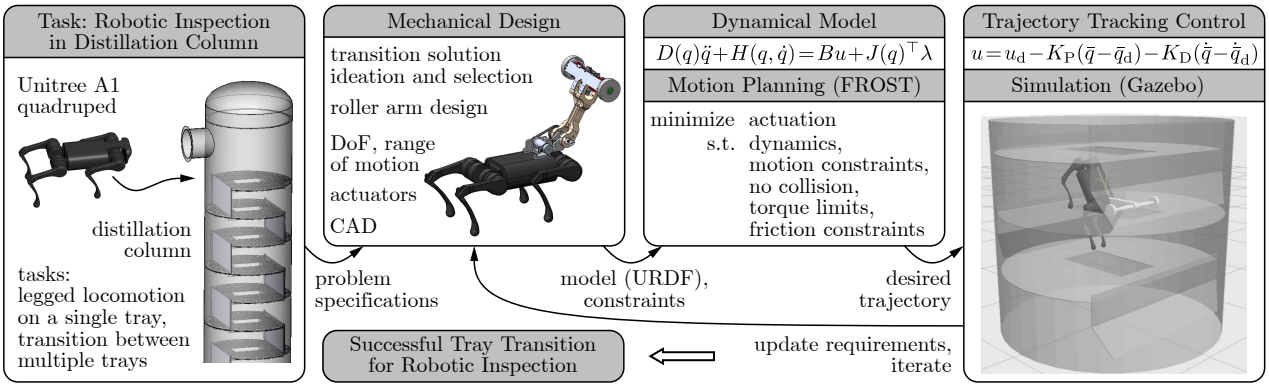

Fig. 1. Overview of robotic mobility system development. The goal is robotic inspection in a distillation column with a quadrupedal robot that needs to transition between the levels (trays) of the column. A roller arm mechanism with appropriate actuators is designed for an off-the-shelf Unitree A1 quadruped that allows tray transition. The model and specifications of the robot are passed down to motion planning that generates a transition trajectory. The trajectory is tracked in high-fidelity simulation where the performance of the system is evaluated. The mechanical design and computation procedures are iterated until successful execution of tray transition.

the column. Examples include a highly dynamic maneuver (jumping) from one tray to next.

- Climbing: part of the robot maintains contact with a tray at all times during transition. For instance, a solution where support legs can grasp onto base tray as other legs extend to the next tray.
- Assisted: the robot uses an additional support mechanism for transition, such as a robotic arm or built-in lift mechanism.

These concepts were evaluated against the design requirements. Infeasible options were eliminated and concepts were down-selected for further analysis. From this analysis (mechanism feasibility, geometric constraints, sequence feasibility and simulation, and dynamic analysis), a legged robot with an added roller arm (shown in Fig. 1) emerged as the leading concept.

The stages of a downward transition using the roller arm are shown in Fig. 3. First, the robot positions itself over the manway. The extender mechanism extends the wheels out and the arm is rotated down so that the wheels establish contact with the tray (first row of Fig. 3). While maintaining contact with the wheels and the rear feet, the robot maneuvers the front legs through the manway and places the front feet on the tray below (second row). The wheel actuators move the arm along the manway during this process. Next, the quadruped shifts its body weight to the front legs while keeping all feet in contact (third row). The rear feet then lift off the upper tray and the legs are maneuvered through the manway onto the lower tray, again with the wheels facilitating any necessary arm travel along the manway (fourth row). Finally, the arm rotates up to break contact between the wheels and tray,

Table 1. Distillation column parameter ranges.

Parameter	Min (in)	Max (in)
Tray Diameter	36	360
Tray Clearance	16	36
Manway Length	22	48
Manway Width	13.5	18

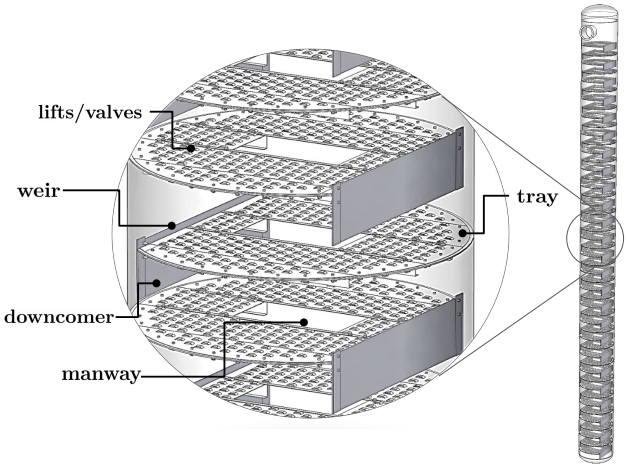

Fig. 2. Illustration of distillation columns and their trays.

the extender is activated to contract the wheels in, and the arm rotates down to sit stowed on top of the robot. To transition up, these steps are followed in reverse order.

To accomplish the tray transition as described, the roller arm mechanism has four actuated degrees of freedom (DoF). The first DoF is the rotation of the main arm

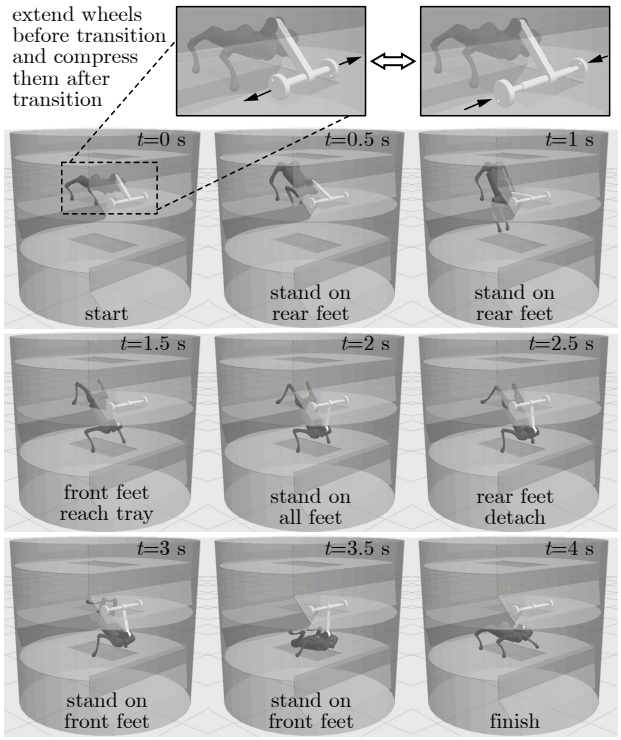

Fig. 3. Tray transition sequence with the roller arm. Before and after transition, the wheels are extended and compressed, respectively. Transition consists of three phases with contact at rear feet (top), all feet (middle) and front feet (bottom).

link. This provides the leverage to lower or raise the robot through the manway. The two actuated wheels move the roller arm and robot along the manway. Each wheel requires its own actuator to robustly roll over the lifts or valves on the trays. Additionally, for a successful transition, it is important to minimize the yaw of the robot relative to the manway, and the independent actuators enable controlling this alignment. Lastly, when a transition is complete the wheels need to be collected so that they can pass through the manway. Several single-DoF concepts were considered, and an extender – using a single actuator to drive right- and left-hand lead screws for a coupled extension or contraction of the wheels – was chosen due to its compactness and ease of operational use.

The roller arm mechanism has several advantages. It maintains contact with trays during the entire transition, minimizing falling risk, and allows for utilization of dynamics to optimize the system (for example with swinging). Additionally, it is completely decoupled from main mobility system, so it can be developed separately and then mounted on a commercial robot, such as the Unitree A1, without requiring modification of the robot.

2.2 Mechanical Design

The roller arm assembly is shown in Fig. 4. The arm is designed to be compatible with tray spacings of 18 to 24 inches, which were identified as the common range in distillation columns. The mass of the arm is about 5 kg (while the Unitree weighs 12 kg). The design is made up of two subsystems: the base and the top of the arm.

The base of the arm is mounted on the robot. It holds the main actuator that is coupled to the arm through a timing belt and drives the arm's rotation, providing the torque to lift or lower the robot's weight. The arm is designed to go through 225 degrees of rotation – from being stowed along the robot's back to being down in front of the robot – and an absolute encoder on the joint of the arm provides rotary position feedback. The maximum required torque on this joint was calculated to be 30 Nm through modeling and simulating the robot and the roller arm in SOLIDWORKS (2019) Motion Analysis. It is desired to sweep through the full arm range of motion in less than 10 seconds, i.e., the joint speed should be greater than 4 rpm. Accordingly, actuators were selected with specifications in Table 2. Note that the pulleys and timing belt add a 2.545 ratio to increase the provided torque, which is especially important after factoring in losses.

The extender mechanism and two wheel assemblies are located at the top of the arm. The extender mechanism is composed of a pair of collinear 1/4"-16 ACME lead screws (left- and right-handed) to allow for extension or contraction of the wheels driven by a single motor. This mechanism can adjust the width of the arm anywhere between 13 and 18 inches, covering the full range of manway widths. The required torque for the extender was calculated as 0.02 Nm using the system and lead screw parameters, with an additional factor of safety. The extender is not designed to function when supporting the full weight of the robot, and it is assumed that it will be functional only when unloaded. The desired time span for a full extension of the wheels was set at 15 seconds, which corresponds to 162.5 rpm lead screw speed. There is an additional gear ratio of 2.5 from a set of spur gears coupling the motor and the lead screw shafts. The exact drivetrain specifications are listed in Table 2. The motor is selected to allow for significantly faster extension and higher nominal torque than the minimum requirements.

Each wheel assembly is coupled with a lead screw and supported with additional linear rails. Assuming the wheels can drive the robot up a 45 degree slope, the wheel actuators need to provide 5 Nm torque (with margin). Additionally, the assumption that the robot can traverse the longest manway length within 4 seconds with a 3 inch diameter wheel results in an actuator output of 58 rpm. The actual system parameters are provided in Table 2.

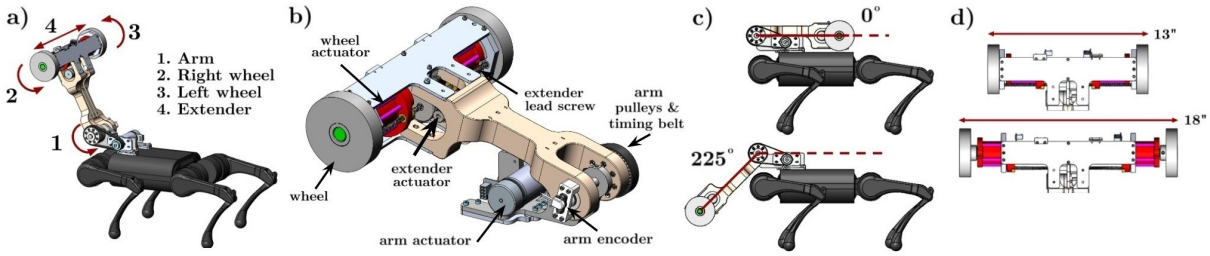

Fig. 4. Specifics of the roller arm mechanical design. (a) The roller arm mounted on the Unitree A1 quadruped and its actuated degrees of freedom, (b) the main components of the roller arm, (c) range of motion of the arm, (d) range of motion of the extender.

Table 2. Specifications of the roller arm.

Joint	Motor & Gear Part No. (Maxon)	Added Gear Ratio	Nominal Output Torque (Nm)	Nominal Output Speed (rpm)
Arm	M651614, G203129	2.545	53.2	11.8
Extender	M267121, G166931	2.5	0.3	230
Wheel	M651607, G203123	-	6.7	70

Finally, the block diagram of the electronics system required to drive the actuators on the roller arm is shown in Fig. 5. It includes two custom printed circuit boards (PCBs) on the arm which incorporate the Maxon EPOS4 motor controller. The motor controllers receive control signals from the computer on-board the robot.

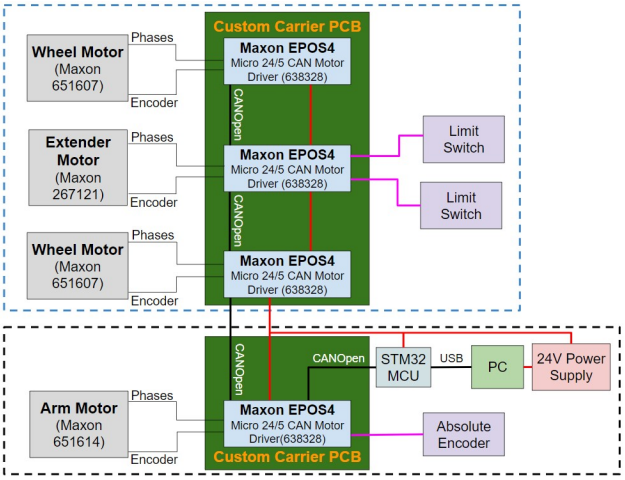

Fig. 5. Roller arm electronics block diagram.

3 MOTION PLANNING AND CONTROL

The roller arm endows the robot with novel dynamic behaviors. Now we describe trajectory generation and tracking for moving up and down in distillation columns.

3.1 Kinematics and Dynamics

The Unitree with the roller arm, shown in Fig. 4, has $n = 22$ DoF, that includes 6 DoF for the body, 12 DoF for the four legs (hip, thigh and knee joints), and 4 DoF for the arm (main arm joint, extender and two wheels). The robot has $m = 16$ actuators, that includes 12 motors on the legs and 4 actuators on the arm. The mechanical model of the robot is constructed based on CAD and stored in Unified Robot Description Format (URDF), as an extension of the Unitree's URDF available at https://github.com/unitreerobotics/.

The model (URDF file) is passed down to motion planning and control, that first generate the forward kinematics and dynamics of the quadruped. We describe the motion with the configuration coordinates $q \in \mathcal{Q}$ evolving in the configuration space $\mathcal{Q} \subset \mathbb{R}^n$. The corresponding velocity coordinates are $\dot{q} \in \mathcal{V}$ in the velocity space $\mathcal{V} \subset \mathbb{R}^n$. The robot is actuated with the control input $u \in \mathcal{U}$ chosen from an admissible input set $\mathcal{U} \subset \mathbb{R}^m$.

When the feet and wheels are in contact with the trays, no-slip conditions are enforced via holonomic constraints of the form $c(q) \equiv 0$ with $c(q) \in \mathbb{R}^k$, where the number k of constraints depends on the number of contact points. The Jacobian of the holonomic constraints is $J(q) = \partial c(q)/\partial q \in \mathbb{R}^{k \times n}$. The motion of the robot is governed by the constrained Euler-Lagrange equations:

$$\begin{aligned} D(q)\ddot{q} + H(q,\dot{q}) &= Bu + J(q)^\top \lambda, \\ J(q)\ddot{q} + \dot{J}(q,\dot{q})\dot{q} &= 0, \end{aligned} \tag{1}$$

where $D(q) \in \mathbb{R}^{n \times n}$ is the mass matrix, $H(q,\dot{q}) \in \mathbb{R}^n$ contains Coriolis and gravity terms, $B \in \mathbb{R}^{n \times m}$ is the actuation matrix, and $\lambda \in \mathbb{R}^k$ is the constraint wrench. This equation is obtained from the URDF using the Fast Robot Optimization and Simulation Toolkit (FROST); see Sec. II.C of [32] for more details on this process.

3.2 Trajectory Optimization

The dynamical model is used for motion planning. Trajectories are generated along which the robot is able

to transition between the levels of the distillation column using its roller arm. The end goal is to find a desired trajectory $q_{\mathrm{d}}(t)$ over a given time interval $t \in [0, T]$ that allows the robot to climb down or up a level safely, without falling into the manway or colliding with the trays.

The transition, illustrated in Fig. 3, consists of three phases: (i) rear feet in contact, (ii) all feet in contact, and (iii) front feet in contact, which have given duration and holonomic constraints. To synthesize this motion, a trajectory is generated via solving an optimization problem using FROST [32]. In continuous time, the optimization problem has the decision variables $X \in \mathcal{X} = C([0, T], \mathbb{R}^{3n+m+k})$, given as follows:

$$X(t) = \begin{bmatrix} q(t)^\top & \dot{q}(t)^\top & \ddot{q}(t)^\top & u(t)^\top & \lambda(t)^\top \end{bmatrix}^\top, \quad (2)$$

which consist of the configuration, velocity, acceleration, torques, and constraint forces over time $t \in [0, T]$.

The optimization problem is formulated as:

$$\begin{aligned} X_{\mathrm{d}} = \underset{X \in \mathcal{X}}{\operatorname{argmin}} \quad & \int_0^T \mathcal{J}(q, \dot{q}, u) \mathrm{d}t \\ \text{s.t.} \quad & D(q)\ddot{q} + H(q, \dot{q}) = Bu + J(q)^\top \lambda \\ & J(q)\ddot{q} + \dot{J}(q, \dot{q})\dot{q} = 0 \\ & h(q) \geq 0 \\ & \lambda \in \mathcal{FC}(q, \dot{q}) \\ & q \in \mathcal{Q}, \;\; \dot{q} \in \mathcal{V}, \;\; \ddot{q} \in \mathcal{A}, \;\; u \in \mathcal{U} \\ & q(0) \in \mathcal{Q}_0, \;\; \dot{q}(0) = 0 \\ & q(T) \in \mathcal{Q}_T, \;\; \dot{q}(T) = 0 \end{aligned} \quad (3)$$

with the following details. The cost $\mathcal{J}$, that is chosen to be the torque of the main arm actuator, $\mathcal{J}(q, \dot{q}, u) = u_{\mathrm{arm}}^2$, is minimized subject to the following constraints:

1. dynamics (1) with holonomic constraints c including: left-right symmetry, fixed wheel extenders, rolling wheels, contact between feet and tray;
2. inequality constraints given by h: no-collision between legs or arm and trays, no self-collisions, angle of contacting legs limited to a given range (so that force sensors at the feet are able to sense contact);
3. friction pyramid constraints $\mathcal{FC}$ with given friction coefficient μ for the feet and wheels in contact;
4. joint angle, velocity, acceleration, and torque limits in the configuration space $\mathcal{Q}$, velocity space $\mathcal{V}$, acceleration space $\mathcal{A}$, and admissible input space $\mathcal{U}$;
5. initial and final configuration in given sets $\mathcal{Q}_0$ and $\mathcal{Q}_T$, implying that all feet are on the selected tray outside the manway, with horizontal body (zero pitch angle), and with zero initial and final velocity.

The optimization problem is solved in discrete time with time step $\Delta t = 0.1\,\mathrm{s}$ using FROST [32]. Note that c, h, $\mathcal{FC}$ and the corresponding dynamics are different for each of the three phases of transition. Accordingly, the robot's motion is expressed as a hybrid system in FROST, with three phases of continuous dynamics (and identity maps connecting these phases). The final outcome of optimization is a desired trajectory $q_{\mathrm{d}}(t)$, associated with velocity $\dot{q}_{\mathrm{d}}(t)$, acceleration $\ddot{q}_{\mathrm{d}}(t)$, torque $u_{\mathrm{d}}(t)$ and constraint wrench $\lambda_{\mathrm{d}}(t)$ over $t \in [0, T]$. The Cartesian coordinates $x_{\mathrm{d}}(t)$, $y_{\mathrm{d}}(t)$ and $z_{\mathrm{d}}(t)$ of the joints and feet are also calculated. The trajectories are stored as a set of waypoints at the time steps $t_i = i\Delta t$, $i \in \{0, \ldots, T/\Delta t\}$.

3.3 Trajectory Tracking

To execute a transition, the offline-optimized trajectory is passed down to a low-level tracking controller. Specifically, we employ a joint-space proportional-derivative feedback controller with torque feedforward:

$$u(t) = u_{\mathrm{d}}(t) - K_{\mathrm{P}}(\bar{q} - \bar{q}_{\mathrm{d}}(t)) - K_{\mathrm{D}}(\dot{\bar{q}} - \dot{\bar{q}}_{\mathrm{d}}(t)), \quad (4)$$

where $\bar{q} \in \mathbb{R}^m$ indicates the actuated DoF that are the last m elements of q (excluding the first $n - m = 6$ floating base DoF), and $K_{\mathrm{P}}, K_{\mathrm{D}} \in \mathbb{R}^{m \times m}$ are control gains.

As the outputs of the trajectory optimization are discrete-time waypoints (at 10 Hz), cubic interpolation is used to produce a continuous reference for $\bar{q}_{\mathrm{d}}(t)$ and $\dot{\bar{q}}_{\mathrm{d}}(t)$. A first-order hold is used for the torque feedforward signal $u_{\mathrm{d}}(t)$ in a similar manner. These interpolated reference signals are transmitted to specific actuators at a 1 kHz where they are tracked onboard via (4) at 40 kHz.

The tracking controller is simulated using a high-fidelity model in Gazebo [33]; see the results in the next section and the video at https://youtu.be/enH0JqkCrGc. The final outcome is the successful, real-time execution of tray transition. While this behavior is crucial for distillation column inspection, note that there exist several other required behaviors (such as stand and walk on a single tray). Therefore, tray transition was encoded as a motion primitive, and it was embedded into the motion primitive framework of [34] that allows the execution of various dynamic behaviors and safe switching from one behavior to another.

Finally, we remark that high-fidelity simulations give insights into, for example, actual torque and power requirements, clearances or collisions between robot and environment, and contact phenomena. These provide feedback for mechanical design, and help further iterate

and optimize the roller arm mechanism. We made the following updates on the design after the simulations:

1. Minor interferences between the robot and the arm (between the front legs, driven pulley and electronics cover) were discovered and removed.
2. The geometry of the arm was optimized to reduce the mass by about 5%, that facilitates dynamic motion under the torque and power constraints.
3. Simulations revealed that delicate electronics components may be close to contact with the tray's edge, hence these components were moved along the arm.
4. More compact motor drivers with custom wire harnesses were installed at a secure location on the arm.

Such design iterations are crucial for executing the transition on hardware, which is our ongoing and future work.

4 NUMERICAL RESULTS

At last, we show the numerical results of the trajectory optimization and high-fidelity simulation.

4.1 Trajectory Optimization

First, we show the trajectories generated by (3) using FROST. We specify the numerical details of this problem below, after a high-level description of the main results.

Figure 6 shows results for a downward tray transition. The geometry of the distillation column and a snapshot illustrating the transition are shown in Fig. 6(a). Side and front views of the transition in the (x, z) and (y, z) planes are depicted in Fig. 6(b,c). The initial and final configurations of the robot are highlighted, the trays are indicated with green lines, and the manway is shown by red lines and dashed black boundary. To illustrate the motion, the spatial trajectories of the body center of mass (blue), front feet (orange), and rear feet (purple) are plotted. Note how the feet are lifted from the upper tray, moved inside and through the manway to the lower tray.

The corresponding angles and velocities of the body pitch, main arm joint and wheels are shown as a function of time in Fig. 6(d,e), whereas the torques of the main arm and wheel actuators are plotted in Fig. 6(f). (Throughout the paper, results are plotted for left joints only due left-right symmetry.) These trajectories are compatible with the joint angle, velocity and torque limits prescribed in the optimization problem (see details below). In the plots, the three phases of transition (with rear feet, all feet, and front feet in contact) are separated by dashed lines. Furthermore, Fig. 6(g) indicates the power exerted by the main arm and wheel actuators ($P_{\mathrm{arm}} = u_{\mathrm{arm}}\dot{q}_{\mathrm{arm}}$ and $P_{\mathrm{wh}} = u_{\mathrm{wh}}\dot{q}_{\mathrm{wh}}$). Notice the higher torque and power requirements when the arm moves significant weight during rear feet contact. Finally, the ratio of friction forces $F_{\mathrm{t}} = \sqrt{F_x^2 + F_y^2}$ to normal forces F_z (extracted from the components of $J(q)^\top \lambda$) is indicated in Fig. 6(h), and it is kept below a given friction coefficient.

To achieve these results, the optimization was set up as follows. The tray clearance was 18 inches, whereas the manway size was 25.5×15 inches. Transition duration was set to $T = 4$ seconds, consisting of 1.5, 1, and 1.5 seconds of rear feet, all feet, and front feet contact. The joint angle, velocity, acceleration, and torque limits in Table 3 were applied. The friction coefficient at the wheels and feet was $\mu = 0.6$. For the legs in contact, the angle of the calf relative to vertical was constrained within $[-75°, 30°]$ to maintain contact between the force sensor at the feet and the tray. Moreover, constraints were imposed on the feet positions to avoid collisions with trays. The feet were lifted vertically to at least 1 inch clearance when detaching from a tray, they were at least 2 inches inside the manway when moving through it, and 2 inches outside when put onto the tray. To avoid collision between the arm and trays, the longitudinal position of the wheels was constrained to stay over the manway, and a 4-inch clearance was prescribed between the main arm joint and the tray edges during the front feet contact phase.

The optimization problem (3) was solved with a fixed number of 100 iterations, hence the resulting trajectories may contain slight constraint violations. For the example of Fig. 6, (1) was violated slightly with a maximum residual of 0.004, while all other constraints were satisfied with residuals less than 0.001 for all time. The residuals could be reduced further by increasing the number of iterations, but we found these results satisfactory for the high-fidelity simulations presented below.

The optimization problem (3) can also generate trajectories for upward transition. In this case, the order of the transition phases is reversed, and the duration of the front feet contact phase was increased to 2 seconds. The resulting trajectory is shown in Fig. 7 (with the same notations as in Fig. 6). The robot starts from the lower tray, pulls its legs inside the manway and maneuvers them to the upper tray (first with a "hand stand" on the front legs and then by standing on its rear legs). In Fig. 7(f,g) we highlight that torque and power are higher in upward transition than downward transition during the rear feet contact phase when the arm is lifting most of the body weight.

Finally, we demonstrate the versatility of the motion planner by generating trajectories for transition across various distillation column geometries. Figure 8 shows downward transition trajectories in four different setups, that include a small (16 inch) and a large (24 inch) tray clearance with a narrow (13.5 inch) and a wide (18 inch) manway. In each case, a collision-free trajectory is generated that is compatible with the optimization constraints.

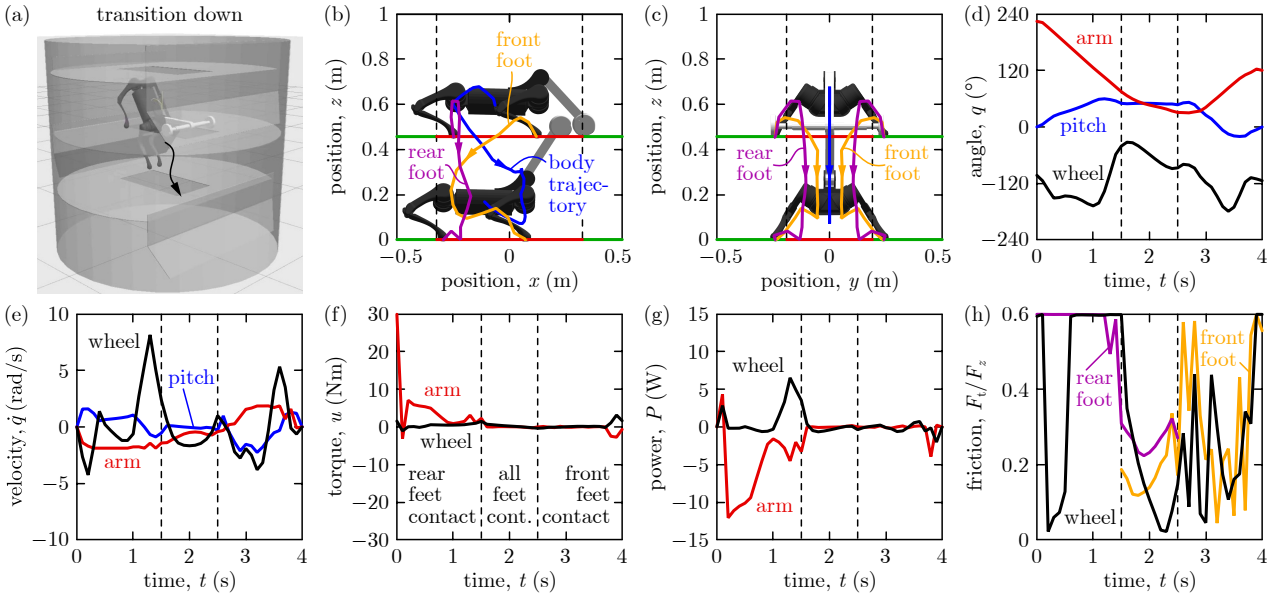

Fig. 6. Trajectory for downward tray transition after solving (3). (a) Illustration of transition, (b,c) body and feet trajectories, (d) evolution of selected joint angles, (e) velocities, (f) torques, (g) power consumption, and (h) ratio of friction and normal forces.

Table 3. Constraints of the optimization problem.

configuration $\mathcal{Q}$	pitch	[-60°, 60°]
	hip	[-46°, 46°]
	thigh	[-60°, 240°]
	knee	[-154.5°, -52.5°]
	arm	[0°, 225°]
	wheel	[-360°, 360°]
velocity $\mathcal{V}$	leg joints	[-21, 21] rad/s
	arm	[-18, 18] rpm
	wheel	[-84, 84] rpm
acceleration $\mathcal{A}$	all joints	[-40, 40] rad/s^2
input $\mathcal{U}$	leg joints	[-33.5, 33.5] Nm
	arm	[-30, 30] Nm
	wheel	[-5, 5] Nm

4.2 High-fidelity Simulation

In this section, we show high-fidelity simulation results, in which the robot tracks the desired trajectory using controller (4) in a Gazebo [33] environment. This allows us to study the tracking performance, as well as validate the generated trajectories. Note that trajectory optimization in FROST was missing some details of the high-fidelity physics (such as sophisticated contact models), which are present in the Gazebo simulation. A video summarizing the simulations can be found at https://youtu.be/enH0JqkCrGc.

Simulation results for downward tray transition are plotted in Fig. 9. The desired trajectories (from Fig. 6) are shown by dashed lines and the actual trajectories are denoted by solid lines. Figure 9(a,b) show body and feet trajectories, whereas Fig. 9(c,d) indicate joint angles. Importantly, transition is successfully executed in high-fidelity simulation despite using simplified model for trajectory generation. Trajectory tracking is accurate for the actuated degrees of freedom $\bar{q}$ (arm, wheel, and leg joints), whereas some discrepancy can be observed for the non-actuated ones (such as pitch angle) that are missing from (4). Similarly, mismatches between the desired and actual positions of the body and feet can be observed, however, these do not affect the success of transition.

Simulation results for upward tray transition are highlighted in Fig. 10. Again, transition is successfully executed, and the tracking performance (relative to the desired trajectory in Fig. 7) is similar to that observed when transitioning down in Fig. 9. We remark that body and feet position errors inevitably arise during transition when using controller (4), since it only considers actuated joint angles and velocities. Position errors could be overcome by more sophisticated tracking controllers, such as those operating in body space rather than joint space. Developing such controllers is left for future work.

As such, note that the simulations above were initiated from the desired initial configuration. In real-life, however, there may be discrepancies in initial conditions. Sensitivity to the initial configuration is studied in Fig. 11 for downward transition. Figure 11(a) shows the transi-

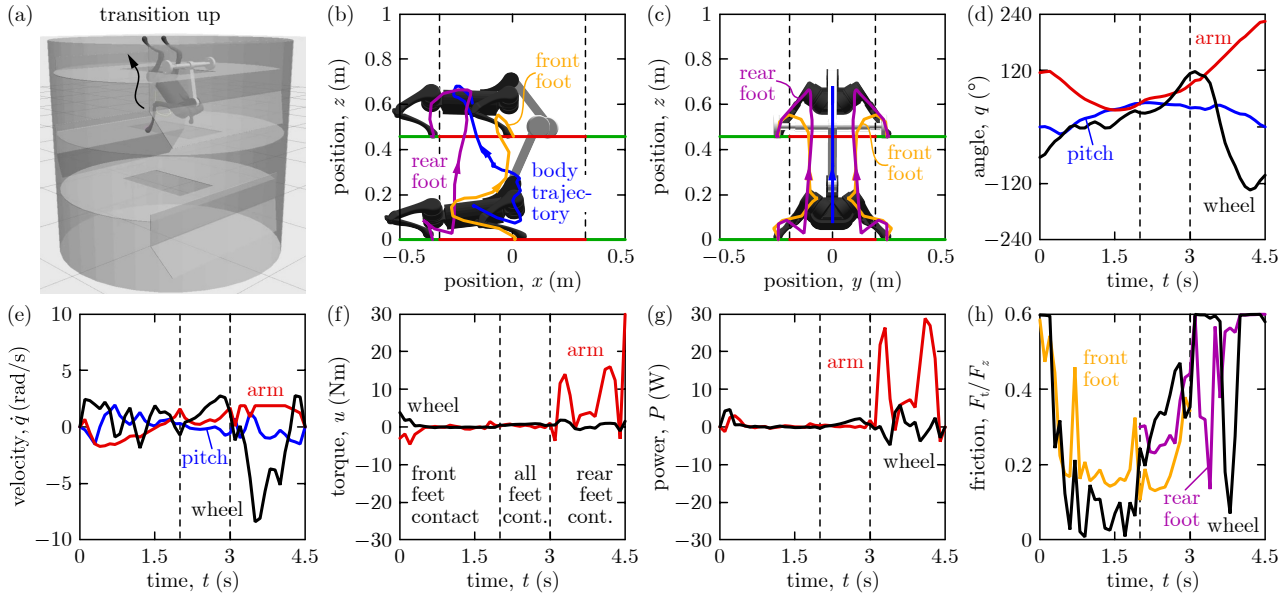

Fig. 7. Trajectory for upward tray transition. Note the higher power requirement for transitioning up compared to transitioning down.

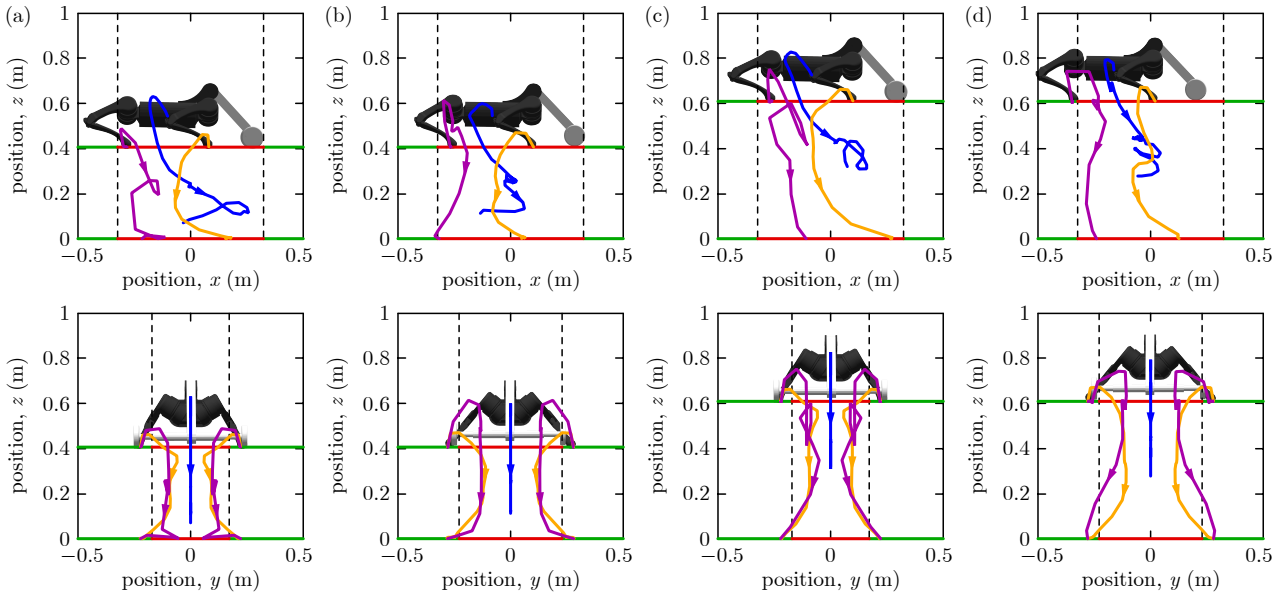

Fig. 8. Trajectories for downward tray transition in various distillation column geometries, with (a,b) small and (c,d) large tray clearance, as well as with (a,c) narrow and (b,d) wide manway.

tion from the desired initial configuration (repeated from Fig. 9), with the desired initial body and feet positions indicated by red color. In comparison, Fig. 11(b,c) demonstrate the effect of ± 5 cm mismatch in initial longitudinal position. Although this causes an undesired offset in body and feet positions throughout the motion, this does not affect the success of transition. Similarly, Fig. 11(d) showcases the effect of a 5-degree initial misalignment between the robot and the manway (i.e., yaw angle error). The transition is successful even with the misalignment, which justifies the robustness of the proposed trajectories.

5 CONCLUSIONS AND FUTURE WORK

In this paper, we developed a robotic mobility platform to execute inspection tasks in distillation columns

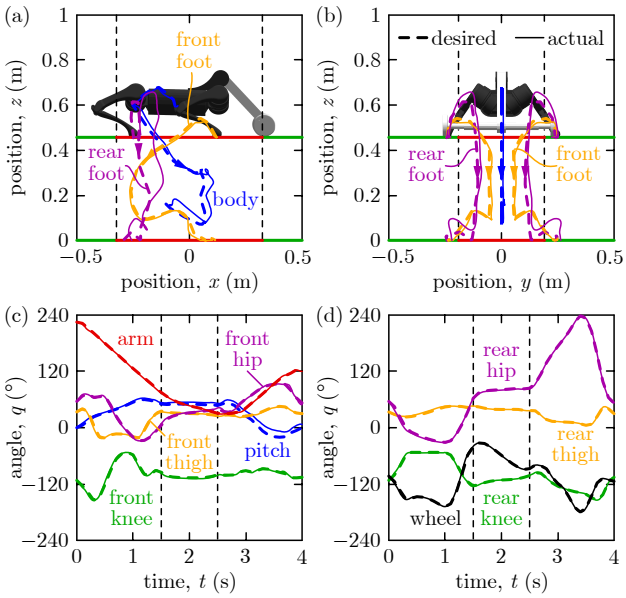

Fig. 9. Simulation results for downward tray transition, wherein the desired trajectory from Fig. 6 (dashed) is tracked by the actual motion (solid). Transition is successful, with accurate tracking at the actuated joints.

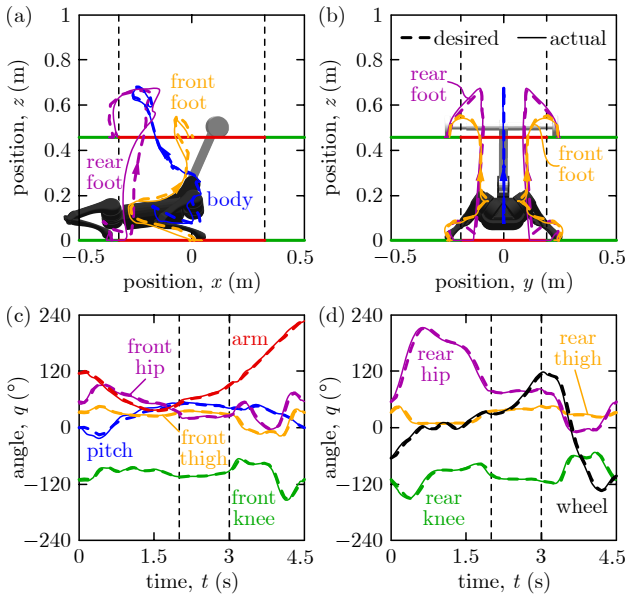

Fig. 10. Simulation results for upward tray transition by tracking the desired trajectory in Fig. 7. The transition is successful in high-fidelity simulation, with similar tracking performance to that of downward transition.

that are dangerous and tedious for humans. A roller arm mechanism was designed and mounted on a quadrupedal robot, and motion planning and control were executed to enable the robot to climb up and down the column. The proposed solution was validated by high-fidelity simulation, and showed success in producing the required behaviors for robotic distillation column inspection.

Our present and future work focuses on prototyping the roller arm and executing the proposed dynamic behaviors on hardware. Implementation requires perception and localization to estimate the quadruped's position inside the column. Furthermore, we plan to improve trajectory tracking, and design safety-critical controllers that prevent collisions or falling into manways by incorporating real-time state estimates into control barrier functions.

ACKNOWLEDGEMENTS

This research is supported by Dow (#227027AT). We would like to thank Lyle McCarty, Twain Pigott, and Marty Robinson from Dow for their insights into distillation column inspection, providing column specifications, and for useful discussions. We would also like to thank Havel Liu from University of Michigan for his great effort and contribution in hardware design and Jay Jasper, Robert Hewitt, and Sarah Etter from NASA Jet Propulsion Laboratory for their valuable ideas and feedback.

The research was in part carried out at the Jet Propulsion Laboratory, California Institute of Technology, under a contract with the National Aeronautics and Space Administration (80NM0018D0004).

REFERENCES

[1] Wong, C., Yang, E., Yan, X.-T., and Gu, D., 2018, "Autonomous robots for harsh environments: a holistic overview of current solutions and ongoing challenges," *Systems Science & Control Engineering,* **6**(1), pp. 213–219.

[2] Takahashi, C., Giuliani, M., Lennox, B., Hamel, W. R., Stolkin, R., and Semini, C., eds., 2021, *Robotics in Extreme Environments* Frontiers Media SA, Lausanne.

[3] Murphy, R. R., Tadokoro, S., Nardi, D., Jacoff, A., Fiorini, P., Choset, H., and Erkmen, A. M., 2008, "Search and rescue robotics," In *Springer Handbook of Robotics*, B. Siciliano and O. Khatib, eds. Springer, Berlin, Heidelberg, pp. 1151–1173.

[4] Pedersen, M. R., Nalpantidis, L., Andersen, R. S., Schou, C., Bøgh, S., Krüger, V., and Madsen, O., 2016, "Robot skills for manufacturing: From concept to industrial deployment," *Robotics and Computer-Integrated Manufacturing,* **37**, pp. 282–291.

[5] Khan, A., Mineo, C., Dobie, G., Macleod, C., and Pierce, G., 2021, "Vision guided robotic inspection

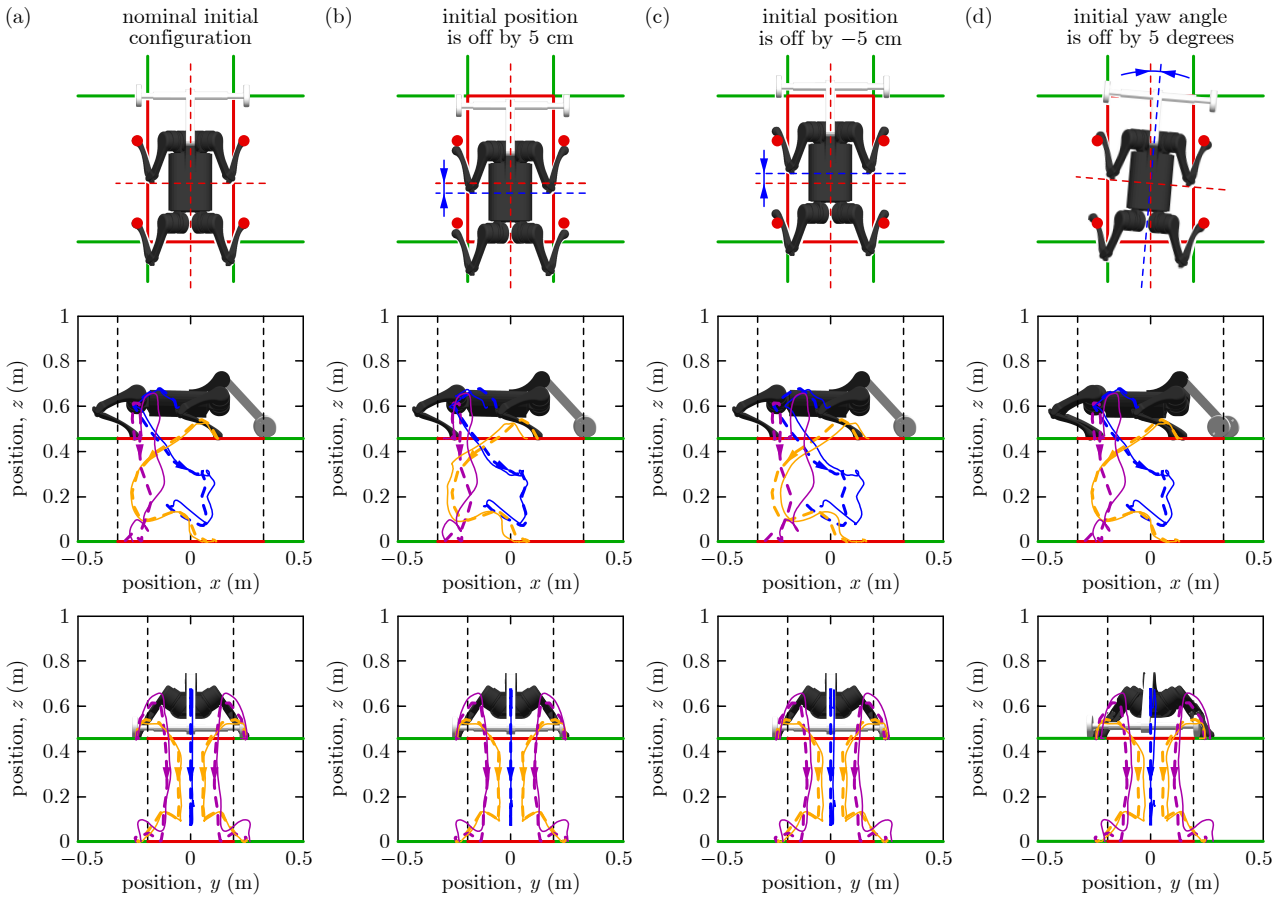

Fig. 11. Analysis of sensitivity to initial conditions in tray transition. Downward transition is started from (a) desired initial conditions, (b) initial longitudinal position 5 cm above desired, (c) 5 cm below desired, and (d) 5 degree initial yaw angle misalignment. Transition is successful in high-fidelity simulation in all cases, that shows robustness to initial position errors.

for parts in manufacturing and remanufacturing industry," *Journal of Remanufacturing,* **11**(1), pp. 49–70.

[6] K., S., 2019, "Automation: Chemistry shoots for the Moon," *Nature,* **568**(7753), pp. 577–579.

[7] Fang, J., and Hunt, K. J., 2021, "Mechanical design and control system development of a rehabilitation robotic system for walking with arm swing," *Frontiers in Rehabilitation Sciences,* **2**(720182), pp. 1–14.

[8] Chignoli, M., Kim, D., Stanger-Jones, E., and Kim, S., 2021, "The MIT humanoid robot: Design, motion planning, and control for acrobatic behaviors," In IEEE-RAS 20th International Conference on Humanoid Robots, pp. 1–8.

[9] Olinski, M., and Ziemba, J., 2014, "Hybrid quadruped robot – Mechanical design and gait modelling," In New Advances in Mechanisms, Transmissions and Applications, V. Petuya, C. Pinto, and E.-C. Lovasz, eds., Springer Netherlands, pp. 183–190.

[10] Yang, J., Jia, W., Sun, Y., Pu, H., Ma, S., Chen, L., and Han, B., 2017, "Mechanical design of a compact and dexterous quadruped robot," In IEEE International Conference on Mechatronics and Automation, pp. 1450–1456.

[11] Bledt, G., Powell, M. J., Katz, B., Di Carlo, J., Wensing, P. M., and Kim, S., 2018, "MIT Cheetah 3: Design and control of a robust, dynamic quadruped robot," In IEEE/RSJ International Conference on Intelligent Robots and Systems, pp. 2245–2252.

[12] Yao, L., Yu, H., and Lu, Z., 2021, "Design and driving model for the quadruped robot: An elucidating draft," *Advances in Mechanical Engineering,* **13**(4), pp. 1–14.

[13] Ur Rehman, B., Focchi, M., Frigerio, M., Goldsmith, J., Caldwell, D. G., and Semini, C., 2015, *Design of a Hydraulically Actuated Arm for a Quadruped Robot* Assistive Robotics. World Scientific, pp. 283–290.

[14] Moran, S., 2017, "Distillation columns and towers," In *Process Plant Layout (Second Edition)*. Butterworth-Heinemann, Oxford, pp. 325–338.

[15] Zhang, Z., Yan, J., Kong, X., Zhai, G., and Liu, Y., 2021, "Efficient motion planning based on kinodynamic model for quadruped robots following persons in confined spaces," *IEEE/ASME Transactions on Mechatronics,* **26**(4), pp. 1997–2006.

[16] Shao, X., Huang, Q., Wang, Z., Cai, Q., and Wang, W., 2014, "Motion planning and compliant control for a quadruped robot on complicated terrains," In IEEE International Conference on Mechatronics and Automation, pp. 1587–1594.

[17] Geisert, M., Yates, T., Orgen, A., Fernbach, P., and Havoutis, I., 2019, "Contact planning for the ANYmal quadruped robot using an acyclic reachability-based planner," In Towards Autonomous Robotic Systems, K. Althoefer, J. Konstantinova, and K. Zhang, eds., Springer International Publishing, pp. 275–287.

[18] Mastalli, C., Havoutis, I., Focchi, M., Caldwell, D. G., and Semini, C., 2020, "Motion planning for quadrupedal locomotion: Coupled planning, terrain mapping, and whole-body control," *IEEE Transactions on Robotics,* **36**(6), pp. 1635–1648.

[19] Ma, W.-L., Csomay-Shanklin, N., and Ames, A. D., 2020, "Quadrupedal robotic walking on sloped terrains via exact decomposition into coupled bipedal robots," In IEEE/RSJ International Conference on Intelligent Robots and Systems, pp. 4006–4011.

[20] Ahn, J., Jorgensen, S. J., Bang, S. H., and Sentis, L., 2021, "Versatile locomotion planning and control for humanoid robots," *Frontiers in Robotics and AI,* **8**(712239), pp. 1–17.

[21] Nguyen, Q., Da, X., Grizzle, J. W., and Sreenath, K., 2020, "Dynamic walking on stepping stones with gait library and control barrier functions," In *Algorithmic Foundations of Robotics XII*, K. Goldberg, P. Abbeel, K. Bekris, and L. Miller, eds. Springer International Publishing, Cham, pp. 384–399.

[22] Csomay-Shanklin, N., Cosner, R. K., Dai, M., Taylor, A. J., and Ames, A. D., 2021, "Episodic learning for safe bipedal locomotion with control barrier functions and projection-to-state safety," In Learning for Dynamics and Control, pp. 1041–1053.

[23] Grandia, R., Taylor, A. J., Ames, A. D., and Hutter, M., 2021, "Multi-layered safety for legged robots via control barrier functions and model predictive control," In IEEE International Conference on Robotics and Automation, pp. 8352–8358.

[24] Lynch, G. A., Clark, J. E., Lin, P.-C., and Koditschek, D. E., 2012, "A bioinspired dynamical vertical climbing robot," *The International Journal of Robotics Research,* **31**(8), pp. 974–996.

[25] Tavakoli, M., and Viegas, C., 2015, "Bio-inspired climbing robots," In *Biomimetic Technologies*, Woodhead Publishing Series in Electronic and Optical Materials. Woodhead Publishing, pp. 301–320.

[26] Elbadawi, M., Andrikopoulos, G., Nikolakopoulos, G., and Gustafsson, T., 2018, "Bio-inspired climbing robots in wet environments: Recent trends in adhesion methods and materials," In IEEE International Conference on Robotics and Biomimetics, pp. 2347–2353.

[27] Schiller, L., Seibel, A., and Schlattmann, J., 2019, "Toward a gecko-inspired, climbing soft robot," *Frontiers in Neurorobotics,* **13**(106), pp. 1–9.

[28] Farzan, S., Hu, A.-P., Davies, E., and Rogers, J., 2019, "Feedback motion planning and control of brachiating robots traversing flexible cables," In American Control Conference, pp. 1323–1329.

[29] Haynes, G. C., Khripin, A., Lynch, G., Amory, J., Saunders, A., Rizzi, A. A., and Koditschek, D. E., 2009, "Rapid pole climbing with a quadrupedal robot," In IEEE International Conference on Robotics and Automation, pp. 2767–2772.

[30] Saputra, A. A., Toda, Y., Takesue, N., and Kubota, N., 2019, "A novel capabilities of quadruped robot moving through vertical ladder without handrail support," In IEEE/RSJ International Conference on Intelligent Robots and Systems, pp. 1448–1453.

[31] Ohara, K., Toda, T., Kamiyama, K., Kojima, M., Horade, M., Mae, Y., and Arai, T., 2018, "Energy-efficient narrow wall climbing of six-legged robot," *ROBOMECH Journal,* **5**(1), p. 26.

[32] Hereid, A., and Ames, A. D., 2017, "FROST: Fast robot optimization and simulation toolkit," In IEEE/RSJ International Conference on Intelligent Robots and Systems, pp. 719–726.

[33] Koenig, N., and Howard, A., 2004, "Design and use paradigms for Gazebo, an open-source multi-robot simulator," In IEEE/RSJ International Conference on Intelligent Robots and Systems, Vol. 3, pp. 2149–2154.

[34] Ubellacker, W., Csomay-Shanklin, N., Molnar, T. G., and Ames, A. D., 2021, "Verifying safe transitions between dynamic motion primitives on legged robots," In IEEE/RSJ International Conference on Intelligent Robots and Systems, pp. 8477–8484.